ORIGINAL RESEARCH

Anti-Inflammatory Immune Skewing Is Atheroprotective: Apoe$^{-/-}$FcγRIIb$^{-/-}$ Mice Develop Fibrous Carotid Plaques

Erin Y. Harmon, PhD; Van Fronhofer, III, PhD; Rebecca S. Keller, PhD; Paul J. Feustel, PhD; Xinmei Zhu, MD, PhD; Hao Xu, BS; Dorina Avram, PhD; David M. Jones, MD; Shanmugam Nagarajan, PhD; Michelle R. Lennartz, PhD

***Background*—**Stroke, caused by carotid plaque rupture, is a major cause of death in the United States. Whereas vulnerable human plaques have higher Fc receptor (FcγR) expression than their stable counterparts, how FcγR expression impacts plaque histology is unknown. We investigated the role of FcγRIIb in carotid plaque development and stability in apolipoprotein (Apo)e$^{-/-}$ and Apoe$^{-/-}$FcγRIIb$^{-/-}$ double knockout (DKO) animals.

***Methods and Results*—**Plaques were induced by implantation of a shear stress-modifying cast around the carotid artery. Plaque length and stenosis were followed longitudinally using ultrasound biomicroscopy. Immune status was determined by flow cytometry, cytokine release, immunoglobulin G concentration and analysis of macrophage polarization both in plaques and in vitro. Surprisingly, DKO animals had lower plaque burden in both carotid artery and descending aorta. Plaques from Apoe$^{-/-}$ mice were foam-cell rich and resembled vulnerable human specimens, whereas those from DKO mice were fibrous and histologically stable. Plaques from DKO animals expressed higher arginase 1 (Arg-1) and lower inducible nitric oxide synthase (iNOS), indicating the presence of M2 macrophages. Analysis of blood and cervical lymph nodes revealed higher interleukin (IL)-10, immune complexes, and regulatory T cells (T_{regs}) and lower IL-12, IL-1β, and tumor necrosis factor alpha (TNF-α) in DKO mice. Similarly, in vitro stimulation produced higher IL-10 and Arg-1 and lower iNOS, IL-1β, and TNF-α in DKO versus Apoe$^{-/-}$ macrophages. These results define a systemic anti-inflammatory phenotype.

***Conclusions*—**We hypothesized that removal of FcγRIIb would exacerbate atherosclerosis and generate unstable plaques. However, we found that deletion of FcγRIIb on a congenic C57BL/6 background induces an anti-inflammatory T_{reg}/M2 polarization that is atheroprotective. **(*J Am Heart Assoc*. 2014;3:e001232 doi: 10.1161/JAHA.114.001232)**

Key Words: atherosclerosis • carotid artery • FcγR • M2 • macrophages • T_{reg}

Stroke is the third leading cause of death in the United States. Each year, ≈600 000 people suffer a first stroke, with 1 death occurring every 4 minutes.[1] Most strokes are ischemic, resulting from rupture of vulnerable carotid plaques. Vulnerable plaques are characterized by accumulation of lipid laden foam cells, large areas of necrosis, and thin or absent fibrous caps.[2] Although atherosclerosis can be medically managed or surgically treated, the pathology responsible for formation of vulnerable versus stable plaques is still unclear. Studying the molecular mechanisms underlying plaque (in)stability requires the use of an appropriate model.

Implantation of a constrictive device around the common carotid artery induces unstable plaques in apolipoprotein (Apo)e$^{-/-}$ and low-density lipoprotein receptor (LDLR)$^{-/-}$ mice.[3–5] Constriction mimics the low, oscillatory flow that, in humans, predisposes sites to atherosclerosis.[6,7] Murine carotid plaques are rich in macrophages (MØ), smooth muscle cells, and lipid[3] and have morphological features (eg, thin cap, necrotic core, reduced collagen area, and intraplaque hemorrhage)[5] characteristic of vulnerable human plaques. Additionally, the carotid artery is amenable to ultrasound biomicroscopy (UBM), allowing plaque development to be followed longitudinally.[7]

Atherosclerosis is a chronic inflammatory disease, highlighting the involvement of the immune system in disease pathology.[8] The involvement of FcγR in atherosclerosis is an active area of research. In humans, vulnerable carotid plaques have increased FcγR expression and are more proinflamma-

From the Centers for Cell Biology and Cancer Research (E.Y.H., V.F., H.X., M.R.L.), Cardiovascular Sciences (R.S.K., M.R.L.), Neuropharmacology and Neuroscience (P.J.F.), and Immunology and Microbial Diseases (D.A., M.R.L.), and Department of Pathology (D.M.J.), Albany Medical College, Albany, NY; Department of Pathology, University of Pittsburgh School of Medicine, Pittsburgh, PA (X.Z., S.N.).

Correspondence to: Michelle R. Lennartz, PhD, Center for Cell Biology and Cancer Research, MC-165, Albany Medical College, 47 New Scotland Ave, Albany, NY 12208. E-mail: lennarm@mail.amc.edu

Received June 27, 2014; accepted October 19, 2014.

tory than their stable counterparts.[9] FcγR bind immunoglobulin G (IgG) monomers or IgG-antigen immune complexes (IC). The activating receptors, FcγRI (CD64) and III (CD16), are expressed in both humans and mice, whereas FcγRIIa and IV are expressed in humans and mice, respectively. Activating FcγR contain cytosolic immunoreceptor tyrosine-based activation motifs that recruit kinases and phospholipases to promote inflammatory responses. The inhibitory receptor, FcγRIIb (CD32), is expressed on B cells and phagocytes. FcγRIIb has a cytosolic immunoreceptor tyrosine-based inhibition motif that recruits phosphatases for dampening of responses.

In mouse models, we and others have shown that Fcγ receptor (FcγR) expression impacts plaque burden.[10,11] Specifically, Apoe$^{-/-}$ mice lacking the FcγR common γ chain have less lipid accumulation in their descending aorta and aortic root than Apoe$^{-/-}$ animals.[10,11] In an LDLR$^{-/-}$ model, aortic root lesions were decreased upon removal of CD16 (FcγRIII).[12] Conversely, removal of the inhibitory FcγRIIb on the Apoe$^{-/-}$ background increases the size of aortic root lesions.[13] Similarly, in an LDLR$^{-/-}$ chimeric mouse model, replacement of the bone marrow with that from FcγRIIb$^{-/-}$ mice exacerbates lesion development in the descending aorta, compared to mice receiving control bone marrow.[14]

How might FcγR expression impact plaque stability? It has been shown that, as IC levels rise, with the associated increase in activating FcγR occupancy, macrophages shift from a pro- to anti-inflammatory phenotype, as evidenced by reduced interleukin (IL)-12 and increased IL-10 production.[15] In vitro, macrophages are plastic, with their polarization state determined by the cytokine environment.[16] Of particular relevance to these studies are the conditions that polarize macrophages toward the anti-inflammatory, wound-healing end of the spectrum. These "alternatively activated" M2 macrophages secrete IL-10, but little IL-12, and are classified as M2a, M2b, or M2c, depending on the polarizing conditions.[17] IL-4 or IL-13 induce M2a macrophages, M2b are generated in response to IC and Toll-like receptor (TLR) engagement, and IL-10 induces the M2c subtype.

Although models, plaque locations, and method vary, most studies agree that a T helper (Th)1/M1 response exacerbates atherosclerosis whereas Th2/M2 polarization is more protective.[18,19] We generated a double knockout (DKO) mouse lacking both Apoe and FcγRIIb to test the role of FcγRIIb in plaque development and stability. The hypothesis was that loss of FcγRIIb would exacerbate the inflammatory response, leading to greater atherosclerosis. We studied of the impact of FcγRIIb expression on plaques in both the descending aorta (a standard mouse model of atherosclerosis) and carotid artery (a more translational and physiologically relevant site for stroke) and report that removal of FcγRIIb dramatically skews the immune system toward the protective, anti-inflammatory end of the spectrum. Specifically, compared to their Apoe$^{-/-}$ counterparts, DKO animals have decreased inflammatory cytokines and elevated IL-10, IC, and regulatory T cells (T_{regs}), indicative of anti-inflammatory skewing. In vitro, stimulation of DKO MØ with lipopolysaccharide (LPS) and IC induces M2 markers IL-10 and arginase 1 (Arg-1) and decreases expression of inducible nitric oxide synthase (iNOS), IL-1β, and tumor necrosis factor alpha (TNF-α), consistent with an M2 MØ phenotype. The result: development of small, fibrous plaques.

Methods

Animals and Diet

All animal procedures were approved by the Albany Medical Center Institutional Animal Care and Use Committee (Albany, NY) and carried out in compliance with National Institutes of Health (NIH) regulations. Apoe$^{-/-}$ mice on the C57BL/6 background were purchased from The Jackson Laboratory (#002052; Bar Harbor, ME) and bred in house. Male mice were used. At 15 weeks, animals were given a Western diet (0.25% cholesterol, 15% cocoa butter, 40% sucrose, TD.08846; Harlan Teklad, Madison, WI), available ad libitum.

Generation of Apoe-FcγRIIb DKO Mice

Apoe$^{-/-}$ mice (#002052; The Jackson Laboratory) were mated with FcγRIIb$^{-/-}{}_{B6}$ (#580, congenic, backcrossed 12 times to C67BL/6; Taconic Farms, Hudson, NY) animals and the F1 progeny (Apoe$^{-/-}$IIb$^{+/-}$) mated to produce Apoe/FcγRIIb DKOs. Genomic DNA was obtained from circulating white blood cells, and DKOs were determined by genotyping using the following primers: oIMR0618: CTCGTGCTTTACGGTATCGCC (mutant); oIMR0619, (common) AAACTCGACC CCCCGTGGATC and oIMR0620, TTGACTGTGGCCTTAAACGTGTAG (wild type; WT).

The polymerase chain reaction (PCR) products: 161 bp (WT) and 232 bp (mutant). This study was reviewed and approved by the institutional animal care and use committee at University of Arkansas for Medical Sciences (former institute of SN).

Cast Devices and Implantation

Conical casts (cone: 0.2×0.1 mm, 1.5 mm in length) were purchased from Promodling BV (The Hague, the Netherlands). Casts were sterilized under UV light (2 hours) and stored in 70% ethanol. Surgeries were performed within 24 hours of sterilization. Casts were placed around the right common carotid artery proximal to the bifurcation, as previously published.[4,7] Briefly, the common carotid artery was exposed

and separated from the vagus nerve. The constrictive device was placed around the artery; casts were tied with a single suture. Animals were housed individually postsurgery.

Ultrasound Biomicroscopy

UBM is a noninvasive technique that allows quantitation of plaque length, percent stenosis, and (as it is done on living animals as a repeated measure) calculation of the rate of plaque progression. Detailed descriptions of the methods, and validation by histological measurements, have been published.[7] Briefly, proper cast placement and altered blood flow were confirmed by UBM 2 weeks postsurgery, at which time baseline images were taken. Ultrasound was performed using the Vevo 770 high-resolution imaging system, as detailed previously.[7] Plaque length was measured using B-mode sagittal views. Plaques length was determined from the UBM images as previously described.[7] Length measurements were of a single continuous plaque, beginning at the proximal cast margin. Percent stenosis was calculated from transverse UBM images using NIH ImageJ software using the following formula:

$$\text{Percent stenosis} = ((A_{IEL} - A_L)/A_{IEL}) \times 100$$

where A_L=the area of the lumen and A_{IEL}=the area circumscribed by the internal elastic lamina.[7] The most stenotic region was reported.

Tissue Harvesting

Nine weeks postsurgery, animals were anesthetized, exsanguinated, and fixed in situ. Exsanguination involved nicking the left ventricle (LV) and the right atrium. A cannula attached to a peristaltic pump was inserted into the LV and the system flushed with cold PBS (1.5 mL/min, 10 minutes). Fixation was accomplished by perfusion with cold 4% formaldehyde/PBS (1.5 mL/min, 10 minutes). The aortic arch and carotid arteries were removed and fixed for 4 hours in 4% paraformaldehyde/PBS. Tissues were transferred to 30% sucrose/PBS overnight at 4°C. Tissue was thereafter transferred to a 1:1 solution of 30% sucrose/PBS/optimal cutting temperature (OCT; 1 hour) and embedded in OCT.

Histology, Immunohistochemistry, and Immunofluorescence

Plaques were sectioned (7 μm) from the proximal end of the cast for 0.6 to 1.0 mm. Fifteen Superfrost Slides (Fisher Scientific, Pittsburgh, PA) were used for each plaque. Sequential sections were put on each slide, such that sections 1 to 15 went on slides 1 to 15. Sections 16 to 30 were placed on slides 1 to 15, respectively, and so on. This generated 15 slides containing multiple sections separated by ≈100 μm and spanning the entire plaque length. Thus, by staining 1 slide (for lipid, collagen, and so on), we obtained information along the entire plaque length. This staining strategy confirmed that the carotid plaques induced proximal to the cast were a single continuous plaque and allowed consistent staining along the entire length of the plaque. Slides were imaged on an Olympus BX51 microscope (Olympus, Tokyo, Japan) equipped with a QImaging Retiga 2000R digital camera (QImaging, Surrey, British Columbia, Canada) and SlideBook software (Intelligent Imaging Innovations, Inc., Denver, CO).

Percent Stenosis

Percent stenosis was calculated with NIH ImageJ software using the following formula:

$$\text{Percent stenosis} = ((A_{IEL} - A_L)/A_{IEL}) \times 100$$

where A_L=the area of the lumen and A_{IEL}=the area circumscribed by the internal elastic lamina as reported.[7] The most stenotic region, representing the most severely compromised area, was reported for each genotype.

Plaque length

Excised carotid arteries were visualized using an Olympus SZ61 stereomicroscope and imaged using an Olympus DP20 camera. Plaque length was measured using digital microcalipers (Fisher Scientific), as previously described.[7]

CD68

Endogenous peroxidase was quenched with 0.3% H_2O_2 (10 minutes, room temperature). Slides were rinsed with PBS and blocked with 0.1% Tween-20, 2% BSA, and 5% goat serum (1 hour). CD68 antibody (FA-11; Abcam, Cambridge, MA) was applied overnight at 4°C (1:100 in blocking buffer). Secondary antibody was goat anti-rat (60 minutes, room temperature; Vector Laboratories, Burlingame, CA). Antibody was visualized using Vector's ABC kit with diaminobenzadine (BD Biosciences, Franklin Lakes, NJ), followed by hematoxylin counterstain.

Arg-1 and iNOS

Slides were dried overnight and fixed in acetone (10 minutes, −20°C), then rehydrated with PBS (10 minutes) and blocked with 0.5% fish gelatin (G-7765; Sigma-Aldrich, St. Louis, MO), 1% BSA, and 0.3% Triton X-100 (blocking buffer, 1 hour, room temperature). Sections were treated with antibodies to Arg-1 (GTX109242, 1:400 in blocking buffer; GeneTex, Irvine, CA) or iNOS (ab15323, 1:50 in blocking buffer; Abcam) overnight at 4°C. Alexa 488–

labeled goat anti-rabbit (A-11034; Invitrogen, Carlsbad, CA) was used as the secondary antibody (1:500, 60 minutes, room temperature). Nuclei were visualized with 4′,6-diamidino-2-phenylindole (1:1000, 15 minutes, room temperature).

Oil Red O

Frozen sections were fixed (10% formalin, 10 minutes), washed with tap water, then 60% isopropyl alcohol (1 minute each). Sections were stained with a 0.3% Oil Red O (ORO)/60% formalin solution (15 minutes). The 60% isopropyl alcohol wash was repeated, followed by a wash with distilled water, and slides were mounted in aqueous mounting media. Percent ORO positive area was quantified using NIH ImageJ. Briefly, images were converted to 32 bit, cropped, and inverted. Thresholds were determined for identification of ORO-positive area and total plaque area. Three to six sections within each plaque, spaced at least 0.1 mm apart, were analyzed and averaged to determine the percent ORO area for each plaque.

$$\%\ \mathrm{ORO}^{+}\mathrm{area} = (\mathrm{ORO}^{+}\mathrm{area}/\mathrm{total\ plaque\ area}) \times 100$$

Picrosirius Red

Frozen sections were fixed in 70% ethanol (3 minutes) and washed with distilled water (3 minutes). Sections were stained with 0.1% Sirius Red/Sigma Direct Red 80 in saturated aqueous solution of picric acid for 1 hour. Sections were washed twice with 0.5% acetic acid (5 minutes), dehydrated with 100% ethanol, cleared with xylene, and mounted with Cytoseal XYL (Richard-Allan Scientific, Kalamazoo, MI). Percent Picrosirius Red–positive area was quantified using NIH ImageJ as described above for ORO.

$$\%\ \text{Picrosirius red area} = (\text{Picrosirius red-positive area}/\mathit{totalplaquearea}) \times 100$$

Trichrome

Slides were fixed in 70% ethanol (2 minutes), rinsed, and incubated in Bouin's fluid (56°C, 1 hour). Sections were sequentially rinsed, stained with Weigert's hematoxylin, rinsed, stained with Biebruch scarlet-acid fuschin, rinsed again, incubated with phosphomolybdic/phosphotungstic acid, and then stained with Aniline Blue (10 minutes each step). Sections were rinsed, incubated in 1% acetic acid (3 minutes), then dehydrated and mounted with Cytoseal XYL (Richard-Allan Scientific).

Plaque vulnerability index

Stability of plaques was assessed by a clinical pathologist, blinded to the genotype of each animal. Three to six sections from each plaque, spaced at least 0.1 mm apart, were analyzed. Plaque stability for each animal was scored using the most vulnerable sections from each plaque.

Necrosis

Necrotic areas were defined from trichrome-stained sections as deep acellular, debris-containing areas within a plaque based on the work of Seiman et al.[20]

$$\%\ \text{Necrotic area} = (\text{necrotic area}/\text{total plaque area}) \times 100$$

Plasma Assays

Cholesterol and triglyceride

Cholesterol and triglyceride (TG) levels were determined using cholesterol and TG assay kits (Cayman Chemical Company, Ann Arbor, MI), according to the manufacturer's instructions.

Immunoglobulin

Plasma IgG, IgM, IgG1, and IgG2a levels were determined using immunoperoxidase-based ELISAs (Immunology Consultants Laboratory, Portland, OR), according to the manufacturer's instructions.

Oxidized LDL

Plasma oxidized LDL (oxLDL) levels were determined by ELISA for oxLDL (Uscn Life Science Inc., Wuhan, China), according to the manufacturer's instructions.

oxLDL-IC

ELISA plates were coated (2 hours, room temperature) and incubated overnight (4°C) with anti-apolipoprotein B antibody (polyclonal; Abcam) diluted 1:750 in PBS. Subsequently, plates were washed with 0.05% Tween-20/PBS and blocked 3 times (10 minutes) with SuperBlock Blocking Buffer/TBS (Thermo Scientific, Waltham, MA). Plasma was diluted 1:500 in diluent buffer (0.1% Tween-20, 10% SuperBlock/TBS) and applied (2 hours, room temperature). Incubation continued overnight at 4°C. Plates were then washed 3 times. Next, a 1:500 dilution of horse anti-mouse IgG (Vector Labs) was added (2 hours, room temperature). The plate was again incubated with streptavidin-HRP (1:1000; BD Biosciences) for 1 hour (room temperature). The plate was washed 3 times, a 1:2 solution of BD Opt EIA TMB Substrate Reagent Set (BD Biosciences) was added, and the reaction was stopped with H_3PO_4 after 2 minutes.

Cytokines

Cytokines were measured using Bio-Plex Custom Luminex® Arrays according to the manufacturer's instructions.

RNA Extraction and Quantitative PCR

Plaques and the associated artery were removed from exsanguinated animals and lysed in Tri-reagent (Molecular Research Center, Cincinnati, OH). Right cervical lymph nodes were homogenized and seeded at 1×10^6 cells/0.75 cm^2. Cells were treated with phorbol 12-myristate 13-acetate (PMA; 20 ng/mL) and ionomycin (1 μg/mL) for 4 hours (37°C). RNA was isolated from Tri-reagent lysed tissues according to the manufacturer's instructions. cDNA was prepared from RNA using iScript (Bio-Rad, Hercules, CA). Qunatitative PCR (qPCR) primers were designed using Primer Express 3.0 (Applied Biosystems, Foster City, CA) to amplify unique sequences (as determined by BLAST analysis) of 100 to 200 bp that crossed an intron. cDNA was amplified using PerfeCta SYBR Green Fast Mix (Quanta BioSciences, Inc., Gaithersburg, MD) with a Step One Plus Real-Time PCR System (Applied Bioscience). Relative expression of each gene was calculated using the ΔΔCt method. Relative abundance of mRNA was normalized to β-actin and calculated as: 2^−(C_t gene−C_t β-actin), where C_t represents the threshold cycle for each transcript. Primers are listed in Table 1.

Flow Cytometry

Cells were blocked with CD16/CD32 (Mouse Fc Block, Clone 2.4G2; BD Pharmingen, Franklin Lakes, NJ) for 15 minutes on ice, then incubated with antibodies to the proteins of interest (45 minutes, on ice). Antibodies were from eBiosciences (San Diego, CA): CD3-PE (phycoerythrin) (clone 145-2C11); CD4-FITC (Clone GK1.5); CD8a-eFluor450 (Clone 53-6.7); CD11b-allophycocyanin (APC)-eFluor780 (Clone M1/70); CD11c-APC (Clone N418); CD45R(B220)-PE-cyanin 7 (Clone RA3-6B2); and major histocompatibility complex (MHC) class II (I-A/I-E)-APC (Clone M5/114.15.2). Staining for FcγRI expression was done using CD64-PE (Clone 290322) from R&D Systems (Minneapolis, MN). Unstained cells were used to establish flow cytometer settings. Single-color positive controls were used for compensation. Flow cytometric data were acquired on a FacsCalibur (Becton and Dickenson, Franklin Lakes, NJ) using FlowJo. The data were analyzed with FlowJo Software (Tree Star, Ashland, OR).

Nuclear Staining for Forkhead Box Protein 3

After surface staining, cells were fixed overnight in Fixation/Permeabilization Buffer (eBiosciences). The following day, cells were permeabilized in permeabilization buffer (eBiosciences) and stained with forkhead box protein 3 (FoxP3)-APC (Clone FJK-16s; eBiosciences) for 30 minutes.

Macrophage Stimulation

Thioglycollate-elicited peritoneal macrophages from Apoe$^{-/-}$ and DKO were obtained 3 to 4 days after injection of 3% thioglycollate (1 mL/mouse). Peritoneal cells (7×10^5 cell/well) were plated in RPMI medium supplemented with 10% IgG-free FBS, 2 mmol/L L-glutamine, 1 mmol/L sodium pyruvate,

Table 1. Primers Used in This Study

Gene	Forward	Reverse
β-actin	TCGCCTGAGGCTCTTTTCC	AGTTTCATGGATGCCACAGGAT
CD64 (FcγRI)	AGATGCTGGATTCTACTGGTGTGA	TGTGAAACCAGACAGGAGCTGAT
CD16 (FcγRIII)	ACTGTCCAAGACCCAGCAACTAC	GCACATCACTAGGGAGAAAGCA
CD16-2 (FcγRIV)	ACAAATCTTCAGCATCCTTTCGTAT	CGGTGGAAACATGGATGGA
SR-A	CAGACTGAAGGACTGGGAACACT	GGAGGCCCTTGAATGAAGGT
CD36	GCCTCCTTTCCACCTTTTGTT	CGTAGATAGACCTGCAAATGTCAGA
Lox-1	GGTTCCCTGCTGCTATGACTCT	GGCGTAATTGTGTCCACTGTACA
Tbet	TACCAGAACGCAGAGATCACTCA	CTCAAAGTTCTCCCGGAATCC
GATA-3	AGAACCGGCCCCTTATCAAG	GACAGTTCGCGCAGGATGT
Foxp3	TCCCACGCTCGGGTACAC	TTGCCAGCAGTGGGTAGGAT
RORγ	AGCGGCTTTCAGGCTTCAT	TCCATTGCTCCTGCTTTCAGT
BCL-6	GCAGAGACTCTTTCGGGCTTT	GATGTGGACTTGGACTCATTCATG
IFN-γ	GGATGCATTCATGAGTATTGC	CCTTTTCCGCTTCCTGAGG
IL-4	GCTGTGAGAATGGGACCTTCTT	AGCGAGGCCTCCTCAGAGA
IL-10	GATTTTAATAAGCTCCAAGACCAAGGT	TTCTATGCAGTTGATGAAGATGTCAA
IL-17a	GGACTCTCCACCGCAATGAA	GCACTGAGCTTCCCAGATCAC

1× nonessential amino acids, and 1× pen/strep. Adherent peritoneal macrophages were used after 48 hours. To determine M1/M2 macrophage polarization, macrophages (5×10^5 cells/well) were treated with BSA-IC (10 μL/well) or LPS (20 ng/mL) plus BSA-IC (10 μL/well) for 6 hours. RNA was isolated and mRNA expression of M1 and M2 marker genes were determined by quantitative real-time PCR (qRT-PCR).

Statistics

Statistical analyses were performed, and graphs constructed, using GraphPad Prism (V.5; GraphPad Software Inc., San Diego, CA) or Origin (v8.1; OriginLab Corporation, Northhampton, MA). The independent sample *t* test was used for all data measured on a continuous scale. For ordinal data (plaque vulnerability index and iNOS/Arg-1 staining score), Mann–Whitney's nonparametric test was employed. Significance was set at $P<0.05$. A hierarchical linear model was used for plaque length and percent stenosis measure. In each animal, a linear regression was used to fit data as a function of time. The slopes for each group (Apoe−/− and DKO) were then compared with a *t* test.

Results

Model for Induction of Carotid Plaques

Placement of a shear stress-modifying cast around the common carotid artery promotes plaque formation proximal to the cast.[3,5,7] UBM pulse-wave Doppler is a noninvasive tool to monitor plaque length and stenosis.[7] Using carotid constriction and UBM in 15- to 26-week-old mice, we determined the effect of FcγRIIb expression on the development and histology of carotid plaques (Figure 1A).

Loss of FcγRIIb Reduces Carotid Stenosis

Plaque length and percent stenosis were followed longitudinally using UBM (Figure 1A). The rate of plaque development, calculated as change in plaque length with time, was not significantly different (Figure 1B). In contrast, stenosis, a clinical metric of plaque risk, was significantly less in DKO plaques (Figure 1C). UBM parameters were validated by direct measurements of plaque length and stenosis (Figure 1D) from 9-week postsurgery tissue. With respect to percent stenosis, values measured by UBM were consistently lower than those obtained postmortem. The likely explanation is that, in live animals, blood pressure keeps the artery lumen more open.

The lower stenosis (with similar plaque length) suggests that DKO mice have less carotid plaque. To determine whether these differences were specific to the carotid artery, we quantified plaque area in the descending aorta using ORO lipid staining.[14,21] Based on this standard measure of atherosclerosis, DKO aortas had less significantly less ORO staining, compared to their Apoe$^{-/-}$ counterparts (Figure 2). Similar results between the carotid and descending aortas suggest that the lower carotid plaque burden in DKO animals is not site specific.

FcγR Expression Affects Plaque Histology

DKO plaques resemble stable human carotid plaques

Guided by American Heart Association criteria,[22] trichrome-stained carotid plaques from Apoe$^{-/-}$ and DKO animals (Figure 3A) were scored for stability. The slides were arbitrarily numbered to obscure the genotype and scored by a pathologist experienced in grading human plaques. (Note: Given that this work assesses mouse plaques for features characteristic of human plaques, we chose the terms "high risk" and "stable," acknowledging that high risk implies likely to rupture, rare in mice.[5])

Multiple sections (3 to 10, depending on plaque length) corresponding to different plaque regions spaced 0.1 mm apart were scored on a 6-point scale, with "1" being no plaque and "6" being lipid rich with little or no fibrosis (Figure 3B). Plaques with subendothelial lipid and buried fibrosis were given higher scores ("5"), whereas more-fibrotic plaques with buried lipid scored lower ("3"). The scores for each region were averaged and plotted. DKO plaques scored significantly lower ($P<0.01$) than Apoe$^{-/-}$, indicative of relative stability (Figure 3B). The differences are still significant if animals with no plaque are excluded from the analysis ($P<0.05$). Given the significant differences in scores, with DKO plaques scored more stable than Apoe$^{-/-}$, histological analyses were done to quantify established indicators of human plaque vulnerability (necrosis, retained lipid, and collagen).

Necrotic area is smaller in DKO plaques

Necrosis is a feature of advanced human plaques and arises from the defective clearance of apoptotic cells[23] (efferocytosis). The combination of a necrotic core and thin/absent cap increases the risk of plaque rupture and stroke in humans.[23] Because there is no direct stain for necrosis, it was inferred from trichrome-stained sections. Intraplaque areas (as reported by Seimon et al.[20]) († in Figure 3A) were scored as necrotic. By this criterion, necrosis was significantly higher in Apoe$^{-/-}$ (Figure 3A and 3C).

DKO plaques have significantly less retained lipid

Plasma levels of cholesterol and TG trended higher in DKO mice, but were not significantly different (Apoe$^{-/-}$:

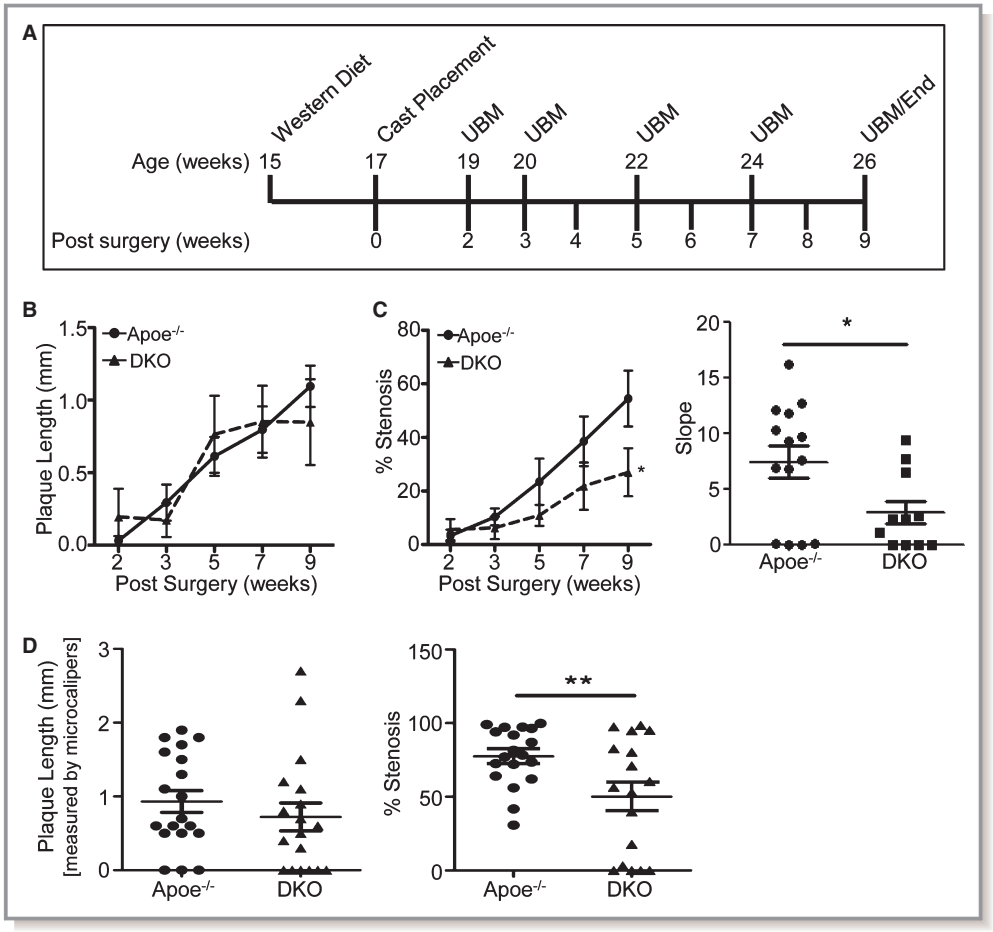

Figure 1. Carotid plaques from DKO mice are less stenotic. A, Study timeline. B, Plaque length and percent stenosis (C) calculated from UBM measurements. The rate of plaque development was calculated by linear regression of data points for each individual animal over time n=11 (DKO) and 14 (Apoe$^{-/-}$). C, The slopes of the percent stenosis change with time were compared and significance determined by independent sample *t* test. **P*<0.05. D, Plaque length measured from postmortem whole mounts and percent stenosis calculated from histological sections of 9 weeks postsurgery tissue. Each symbol represents 1 plaque. Data analyzed by independent sample *t* test. n=18 (DKO) to 19 (Apoe$^{-/-}$). ***P*<0.01. Apo indicates apolipoprotein; DKO, double knockout; UBM, ultrasound biomicroscopy.

1345±157 and 106±16; DKO: 1703±362 and 175±50, respectively, mean±SEM, n=7 to 9). However, quantitation of ORO-positive area revealed significantly less overall lipid in DKO plaques (Figure 4A). Moreover, average lipid inclusion size was significantly smaller in DKO plaques (Figure 4A). Differences in retained lipid could result from alterations in uptake. Thus, we quantified scavenger receptor class A (SR-A), CD36, and lectin-like oxidized low-density lipoprotein receptor 1 (Lox-1) receptor expression in plaques. SR-A and Lox-1 message levels were similar (Figure 4B); CD36 levels were elevated in DKO plaques. Paradoxically, up-regulation of CD36 would be expected to *increase* lipid retention and thus cannot explain the significantly smaller lipid inclusions present in DKO plaques. It is possible that uptake through different receptors or alterations in cholesterol efflux vary between the genotypes.

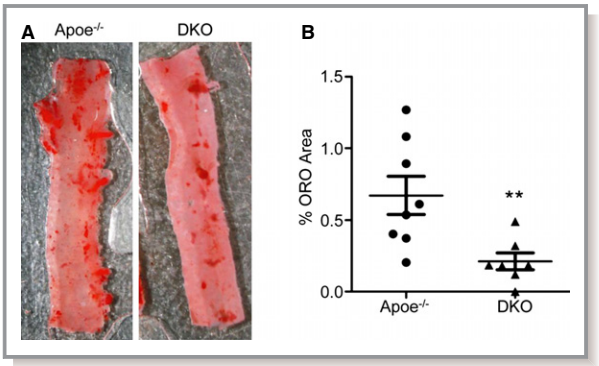

Figure 2. Oil red O (ORO) staining is significantly less in double knockout (DKO) descending aortas. A, Representative thoracic aortas from apolipoprotein (Apo)e$^{-/-}$and DKO mice stained with ORO. B, % ORO positive area; each symbol represents 1 plaque (7 DKO; 8 Apoe$^{-/-}$). Data were analyzed by independent sample *t* test. ***P*<0.01.

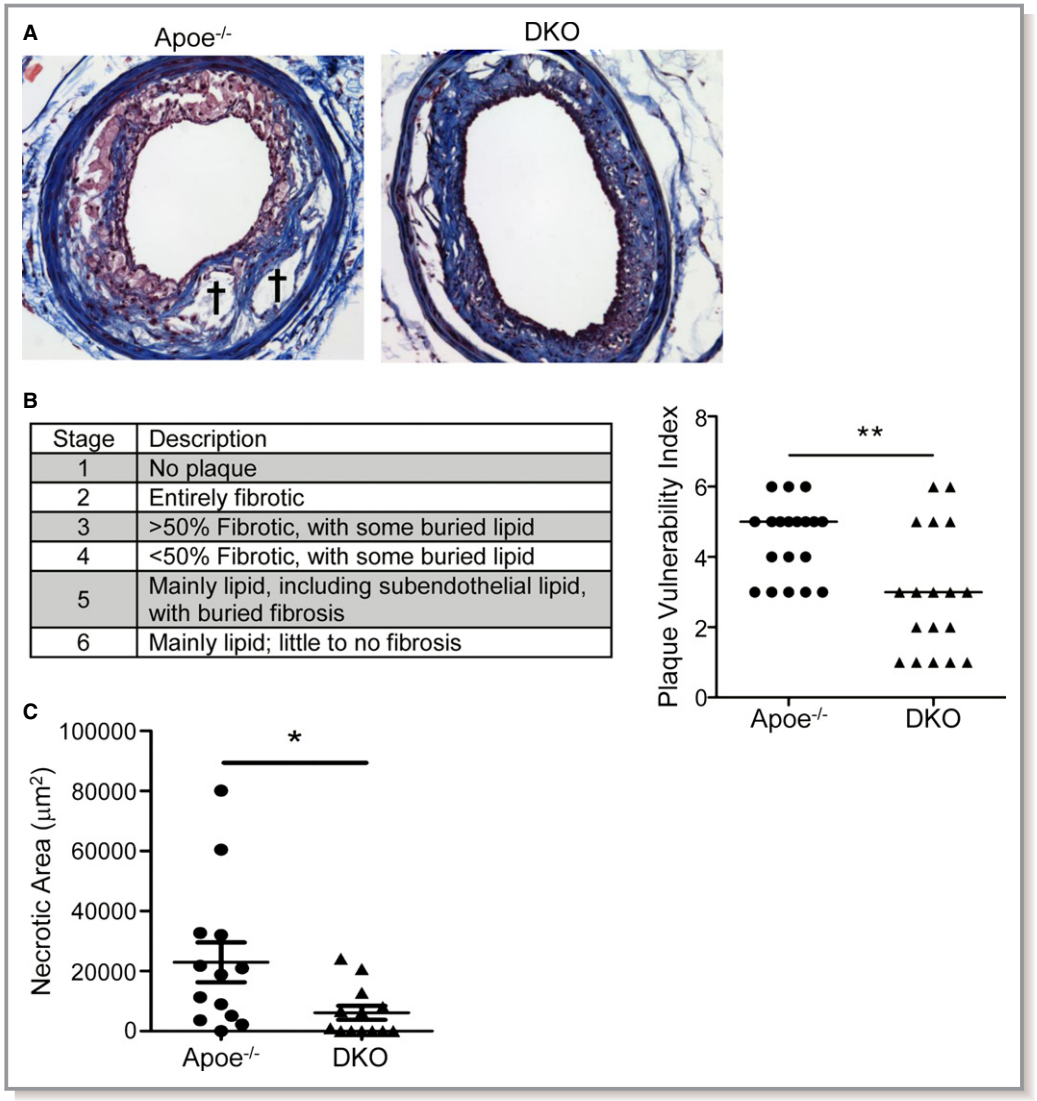

Figure 3. Plaques in double knockout (DKO) mice are more stable. A, Representative trichrome-stained plaques. †Necrotic regions. B, Plaque scoring scale (left) and data (right). Group ranks were significantly different by Mann–Whitney's nonparametric test; $^{**}P<0.01$. C, Quantitation of necrotic area. Data (mean±SEM) analyzed by independent sample *t* test; $^{*}P<0.05$. B and C, Each symbol represents 1 animal. n=18 (DKO) or 19 (Apoe$^{-/-}$). Apo indicates apolipoprotein.

DKO plaques have fibrous caps

Quantification of Picrosirius Red staining (as a percentage of plaque area) established that the amount of collagen in Apoe$^{-/-}$ and DKO plaques was similar (Figure 5A). However, a comparison of the matrix stained either with trichrome (blue in Figure 3A) or Picrosirius Red (Figure 5A) revealed difference in its *distribution*. Specifically, matrix was localized beneath foam cells in the majority of Apoe$^{-/-}$ plaques. Quantitatively, 58% of Apoe$^{-/-}$ and 36% of DKO plaques (11 of 19 and 5 of 13, respectively; Figure 3B) had buried caps (stage 5) or little/no fibrosis (stage 6). In contrast, collagen was concentrated in thick caps (Figure 5A and 5B) and/or throughout the plaque (Figures 3A and 5) in the majority (8 of 13; 62%) of DKO plaques. In humans, superficial collagen protects the fatty/necrotic core, favoring stabilization. In contrast, collagen buried beneath ORO^{+} areas exposes the foam cells to the vessel lumen and increases vulnerability.[24]

Differential Macrophage Polarization in Apoe$^{-/-}$ and DKO Animals

An obvious explanation for the fibrous nature and reduced foam cells in DKO plaques would be the absence of macrophages (MØ). CD68 immunostaining established that CD68^{+} cells were present in all Apoe$^{-/-}$ plaques and were subendothelial (Figure 5B). In contrast, 5 of 18 (28%) DKO

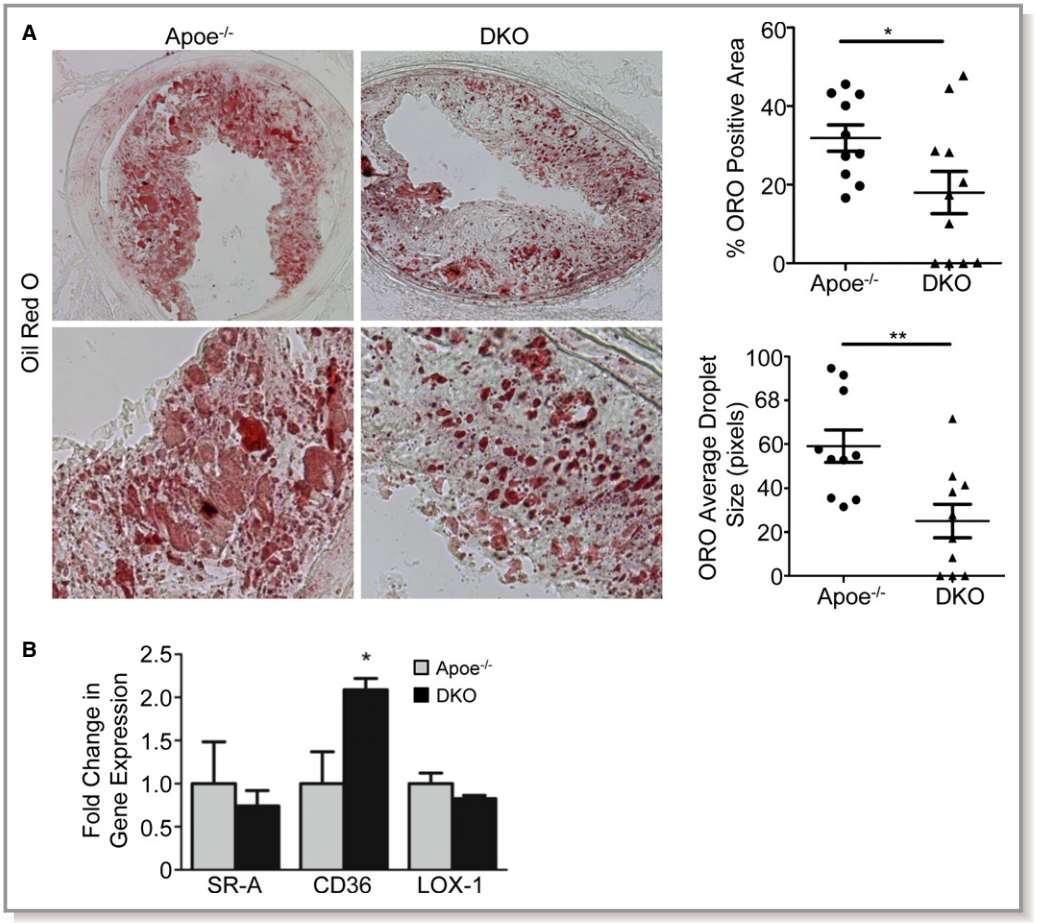

Figure 4. Double knockout (DKO) plaques have less lipid. A, Representative Oil Red O (ORO)-stained plaques showing lipid distribution. Quantitation of overall ORO-positive area and the size of individual lipid-positive foci; n=10 (Apoe$^{-/-}$) to 11 (DKO). B, Relative mRNA expression of scavenger receptors in carotid plaques; n=5 (DKO) to 6 (Apoe$^{-/-}$). Data (mean±SEM) analyzed by independent sample *t* test, **P*<0.05; ***P*<0.01. Apo indicates apolipoprotein; LOX-1, lectin-like oxidized low-density lipoprotein receptor 1; SR-A, scavenger receptor class A.

mice had no plaque (Figure 2B) and 2 of 18 (11%) had plaques with no CD68$^+$ cells. The remaining 11 contained CD68$^+$ cells that were, for the most part, embedded in matrix (Figure 5B). qRT-PCR for CD68 in plaques was similar (Figure 5B). Given that its expression was normalized to β-actin, the results suggest that the percentage of macrophages is similar regardless of plaque size and is consistent with what has been reported for human carotid plaques.[9] Thus, differences in the percentage of MØ cannot explain the fibrotic nature of the DKO plaques.

Histologically, large macrophages (MØ) with expanded ORO-positive cytoplasm (foam cells) and smaller MØ have been associated with pro- (M1) and anti-inflammatory (M2, M_{hem}, and M_{ox}) polarization, respectively.[25,26] M1 polarized MØ express iNOS, whereas M2 synthesize Arg-1 (reviewed previously[27]). If the MØ in Apoe$^{-/-}$ plaques are M1 polarized, they should preferentially express iNOS. Conversely, DKO MØ should be enriched for Arg-1. Three sections of each plaque were stained for iNOS or Arg-1. The slides were given arbitrary numbers and scored by a lab mate blinded to both the genotype and identity of the stained protein. When the code was broken and the averages calculated, Apoe$^{-/-}$ plaques had significantly higher iNOS and lower Arg-1 (Figure 6A), suggesting M1 and M2 polarization of Apoe$^{-/-}$ and DKO plaque MØ, respectively.

Additionally, expression of IL-10, transforming growth factor beta (TGF-β) and TNF-α within the plaques was quantified (Figure 6B). Although IL-10 (anti-inflammatory) trended higher and TNF-α (proinflammatory) trended lower in DKO plaques, the differences, although not significant, were similar to those in the blood (see below) and are consistent with an overall M2/anti-inflammatory environment.

In summary, multiple histological measures provide evidence that DKO carotid plaques share features of stable human plaques and that removal of FcγRIIb attenuates carotid

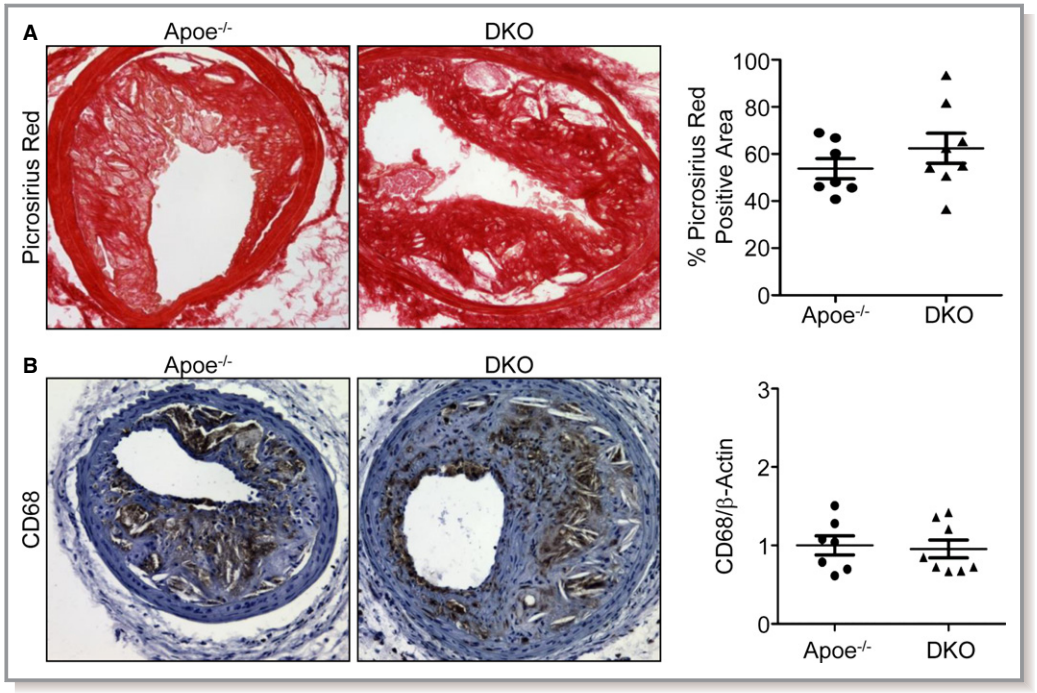

Figure 5. Apoe$^{-/-}$ and DKO plaques are similar with respect to collagen and macrophage content. A, Picrosirius Red staining for collagen. Representative images (left) and quantitation (right) of Picrosirius Red–positive area in individual plaques. B, CD68 staining for macrophages. Although CD68 expression was similar, CD68^{+} cells were superficial in Apoe$^{-/-}$ plaques; most staining was beneath a fibrous cap in DKO samples. (Left) Representative of 14 of 14 Apoe$^{-/-}$ and 11 of 18 DKO animals (excluding DKO animals with no plaque and DKO plaques with no macrophages). (Right) CD68 levels within plaques were assessed by qRT-PCR. Quantitation of Picrosirius Red area and CD68 gene expression is reported as mean±SEM; each symbol represents a single plaque. n=7 (Apoe$^{-/-}$) or 8 (DKO). Significance was evaluated by independent sample *t* test; groups are not significantly different. Apo indicates apolipoprotein; DKO, double knockout; qRT-PCR, quantitative real-time polymerase chain reaction.

plaque development. Immunostaining suggests that DKO plaques express M2 MØ, whereas those from Apoe$^{-/-}$ animals are more M1 polarized, providing a potential explanation for the differences in plaque histology. Because MØ polarization is a function of environment, we interrogated immune tissues for evidence of skewing.

DKO Blood Contains Markers of Anti-Inflammatory Skewing

There were no significant differences in the major circulating cell populations (Table 2). We quantified cytokine levels as a readout of systemic immune polarization. Although there were no significant differences in IL-4 or interferon-gamma (IFN-γ), IL-10 trended higher, and TNF-α, IL-1β, and IL-12 were significantly lower in DKO plasma (Figure 7). The IL-10/IL-12 ratio, an indicator of inflammatory status, was significantly higher in DKO versus Apoe$^{-/-}$ (6.8±1.7 vs. 1.4±0.4, mean±SEM, n=8; $P<0.01$). Elevated IL-10/IL-12 is consistent with atheroprotection given that plaques that develop in an IL-10-rich environment contain small lipid inclusions, minimal necrosis, and thick fibrous caps, all features of stable human, and our DKO, plaques (Figures 4 through 6 and previous works[3,28–30]).

FcγRIIb (single) knockout mice have elevated serum IgG.[31] Similarly, IgG levels were significantly higher in the Apoe$^{-/-}$IIb$^{-/-}$ DKOs at both 15 (chow diet) and 26 weeks (9 weeks on Western diet; Figure 8). The IgG1/IgG2a ratio, an indicator of Th2-Th1 balance, was significantly higher in DKO plasma (39±7 vs. 13±4, n=6; $P<0.05$), consistent with an anti-inflammatory bias. oxLDL was elevated in DKO blood as were the levels IgG/ApoB immune complexes (Figure 8). Given that high IC can shift MØ in an anti-inflammatory (M2) direction,[15] the higher IC in DKO mice is consistent with an anti-inflammatory environment.

MØ From DKO Animals Are M2 Polarized

To examine the effect of FcγRIIb expression on the response of MØ to IC, peritoneal MØ from Apoe$^{-/-}$ and DKO mice were stimulated with IC or LPS+IC and M1 and M2 cytokines were measured. IC induced significantly more

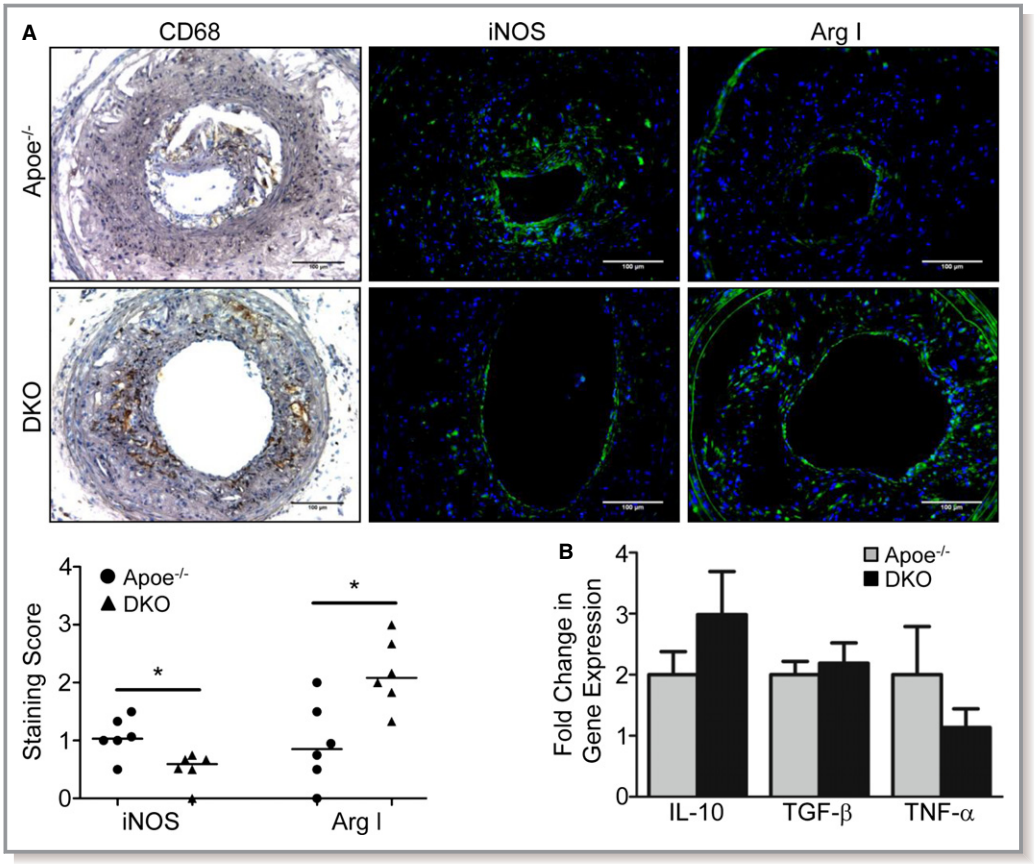

Figure 6. DKO plaques contain M2-polarized macrophages. Representative images of CD68 (macrophages), iNOS (M1), and Arg-1 (M2) staining in DKO and Apoe$^{-/-}$ plaques; scale bar=100 μm. Staining score: 3 sections from each plaque were stained for iNOS or Arg-1. Staining was scored on a 0 to 3 scale (see Methods) for each protein and the averages plotted; each symbol represents the average score from 1 plaque. Group ranks were significantly different (iNOS lower, and Arg-1 higher, in DKO plaques) by Mann–Whitney's nonparametric test; *P<0.05. (B) Expression of IL-10, TGF-β, and TNF-α in plaques was quantified by qRT-PCR. Data are presented as mean±SEM for 4 (Apoe$^{-/-}$) or 5 (DKO) plaques. There were no significant differences between genotypes (independent sample t test). Apo indicates apolipoprotein; Arg-1, arginase 1; DKO, double knockout; IL, interleukin; iNOS, inducible nitric oxide synthase; qRT-PCR, quantitative real time-polymerase chain reaction; TGF-β, transforming growth factor beta; TNF-α, tumor necrosis factor alpha.

Arg-1, and less TNF-α and iNOS, from DKO MØ (Figure 9). The response to LPS and IC was more dramatic, with reduced M1 (iNOS, TNF-α, and IL-1β) and higher M2 (IL-10 and Arg-1) markers (Figure 9A). Quantitation of IL-10 and IL-12 in the media paralleled the qRT-PCR results, with IL-10 significantly higher, and IL-12 lower, in DKO versus Apoe$^{-/-}$ MØ (Figure 9B). The LPS/IC conditions mimic an in vivo environment where dietary lipids ligate TLR4[32,33] and IC cross-link FcγR.

It is possible that deletion of FcγRIIb on the Apoe$^{-/-}$ background could impact macrophage signaling through other FcγR family members (eg, FcγRI, III, or IV). There was no difference in surface expression of FcγRI (CD64) by flow cytometry (Figure 10A), the only receptor for which there are specific antibodies. qRT-PCR revealed no significant differences in message levels for FcγRI (CD64), FcγRIII

Table 2. Cell Composition in Peripheral Blood of Apoe$^{-/-}$ and DKO Mice

Peripheral Blood	Apoe$^{-/-}$ (n=6)	DKO (n=6)
B220^{+}/CD3^{-}	19.5±2.5	23.2±2.1
CD3^{+}/B220^{-}	7.6±0.9	8.2±0.7
CD4^{+}/CD8^{-}*	48.5±2.0	51.9±7.1
CD8^{+}/CD4^{-}*	33.5±6.4	36.5±2.9
CD11c^{+}/CD11b^{+}/CD3^{-}/B220^{-}	6.1±0.8	9.3±2.8
CD11c^{-}/CD11b^{+}/CD3^{-}/B220^{-}/SSC^{hi}	16.9±4.4	23.9±2.0
CD11c^{-}/CD11b^{+}/CD3^{-}/B220^{-}/SSC^{low}	12.0±5.1	13.3±3.9

Analysis of flow cytometric data of peripheral blood of 26-week animals. Data are presented as mean±SEM percent of the total cell population. Data were analyzed by independent sample t test. No significant differences were found. Apo indicates apolipoprotein; DKO, double knockout.
*Percent of CD3^{+} population.

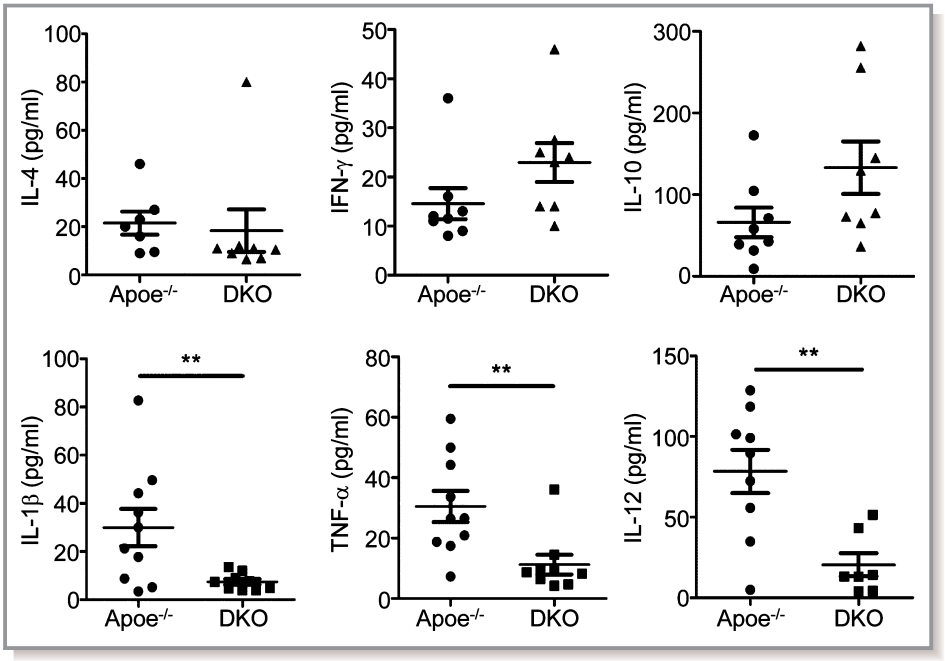

Figure 7. Proinflammatory cytokine levels are significantly lower in DKO plasma. Plasma cytokines were quantified by Luminex® assay. Proinflammatory cytokines TNF-α, IL-1β, and IL-12 were decreased, whereas IL-10 trended higher, in DKO (n=8), compared to Apoe$^{-/-}$ (n=7). Each symbol represents 1 animal. Data are presented as mean±SEM with significance determined by independent sample *t* test $^{**}P<0.01$. Apo indicates apolipoprotein; DKO, double knockout; IFN-γ, interferon-gamma; IL, interleukin; TNF-α, tumor necrosis factor alpha.

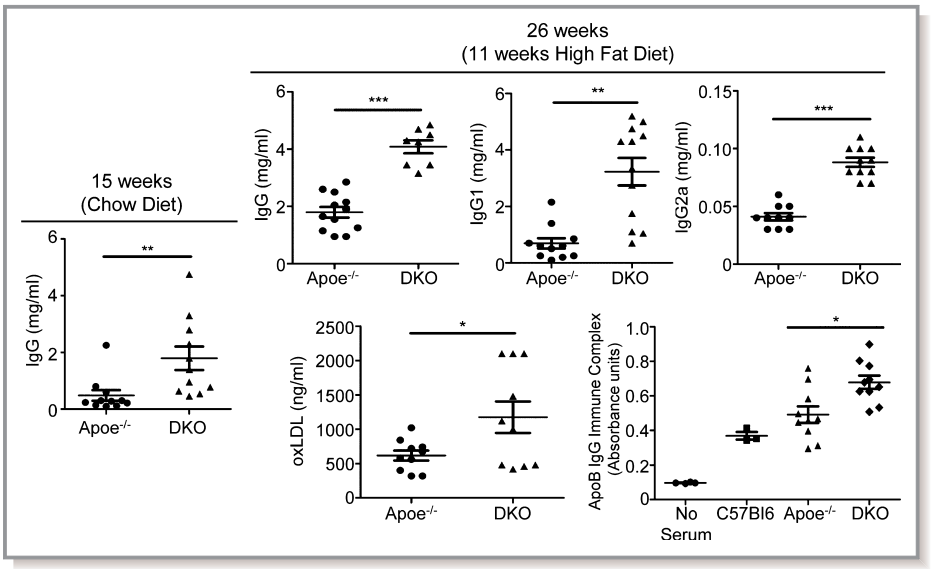

Figure 8. IgG and ApoB immune complexes are higher in DKO plasma. IgG levels in peripheral blood were compared at 15 (chow diet) and 26 weeks (15 weeks chow, 11 weeks high-fat diet). In DKO plasma, all classes of IgG, as well as the concentrations of oxLDL and ApoB-IgG immune complexes, were elevated, compared to Apoe$^{-/-}$. For immune complex levels, the assay controls contained either no serum or serum from 26-week C57/BL6 mice on chow diet. The IC concentration was significantly higher in DKO, compared to Apoe$^{-/-}$, plasma. Each symbol represents 1 animal. Data are presented as mean±SEM for 12 (Apoe$^{-/-}$) and 10 (DKO) animals. Significance was determined by independent sample *t* test. $^{*}P<0.05$; $^{**}P<0.01$; $^{**}P<0.001$. Apo indicates apolipoprotein; DKO, double knockout; IC, immune complexes; IgG, immunoglobulin G; oxLDL, oxidized low-density lipoprotein.

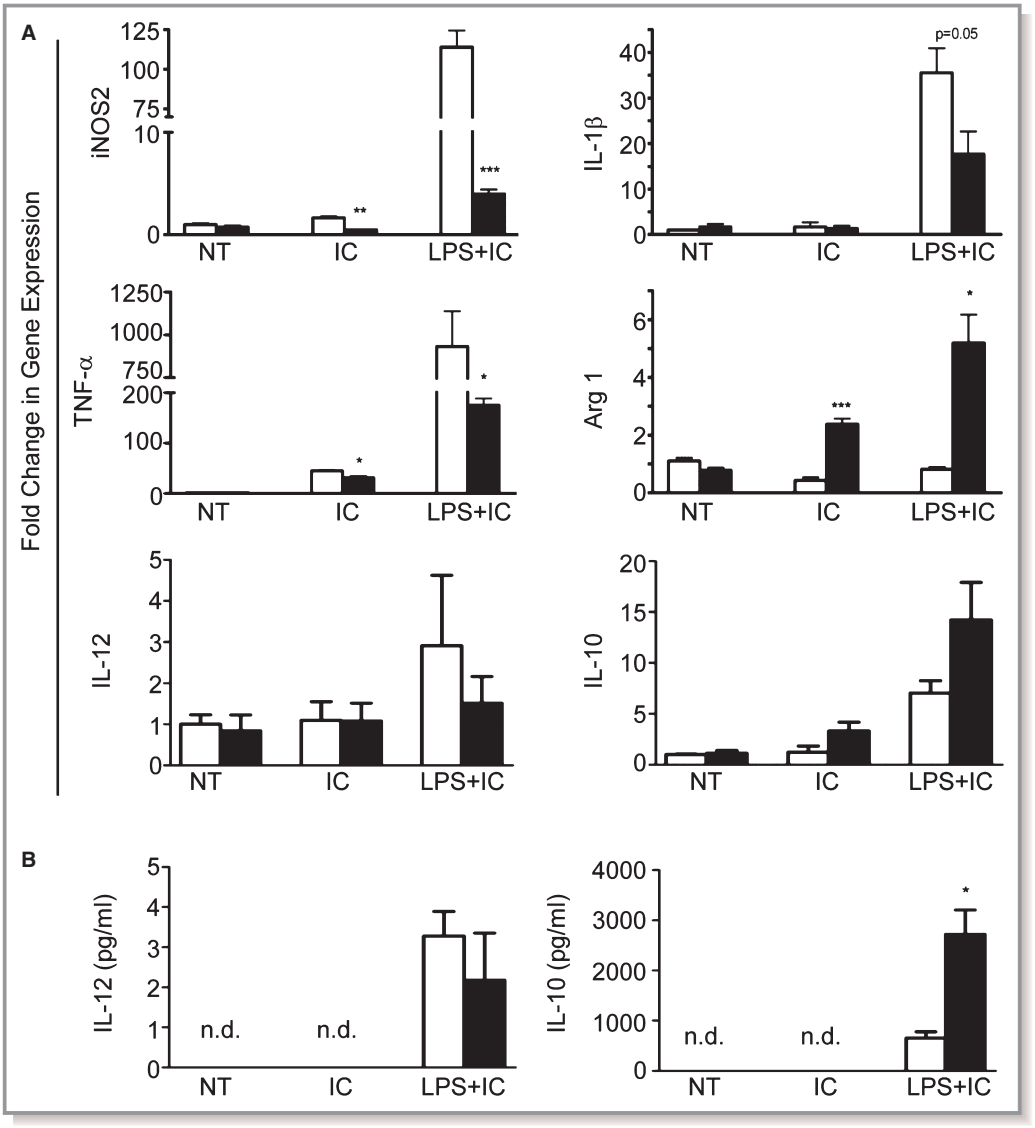

Figure 9. Immune complexes induce M2 polarization in DKO MØ. Peritoneal macrophages were not treated (NT) or stimulated with immune complexes (IC) or LPS+IC (6 hours). RNA was isolated and quantified by qRT-PCR. B, Protein levels of IL-10 and IL-12 from the media of samples in (A). Apoe$^{-/-}$ white bars, DKO black bars (n=3). Significance was determined by independent sample *t* test. n.d., not detected. **P*<0.05; ****P*<0.001. Apo indicates apolipoprotein; Arg-1, arginase 1; DKO, double knockout; IL, interleukin; iNOS, inducible nitric oxide synthase; LPS, lipopolysaccharide; qRT-PCR, quantitative real-time polymerase chain reaction; TNF-α, tumor necrosis factor alpha.

(CD16-1), or FcγRIV (CD16-2) (Figure 10). Additionally, we examined FcγR function by assessing IgG-mediated phagocytosis. Using our published protocol,[34] we calculated the rate of phagocytosis in Apoe$^{-/-}$ and DKO bone marrow-derived macrophages and found no significant difference between the 2 genotypes (Apoe$^{-/-}$: 44.2±2.4 s/target, DKO: 46.6±1.7 s/target, mean±SEM, n=19 events). Thus, we conclude that removal of FcγRIIb has little, if any, effect on the ligation of FcγR, and thus alterations in FcγR expression cannot account for the phenotypic differences between the genotypes.

Lymph Nodes of DKO Animals Suggest T_{reg} Skewing

The interplay between the lymph nodes and tissues allowed us to interrogate the plaque environment by analyzing the cervical lymph nodes draining the casted artery. CD4$^+$ cells, notably CD4$^+$Foxp3$^+$ T_{regs}, were a higher percentage of the total CD3 cell population in DKO animals (Figure 11A and Table 3). CD4$^+$Foxp3$^+$ T_{regs} contribute to atheroprotection[35,36] and are linked to plaque stability in humans.[37] In addition, the percentage of antigen-presenting cells, that is,

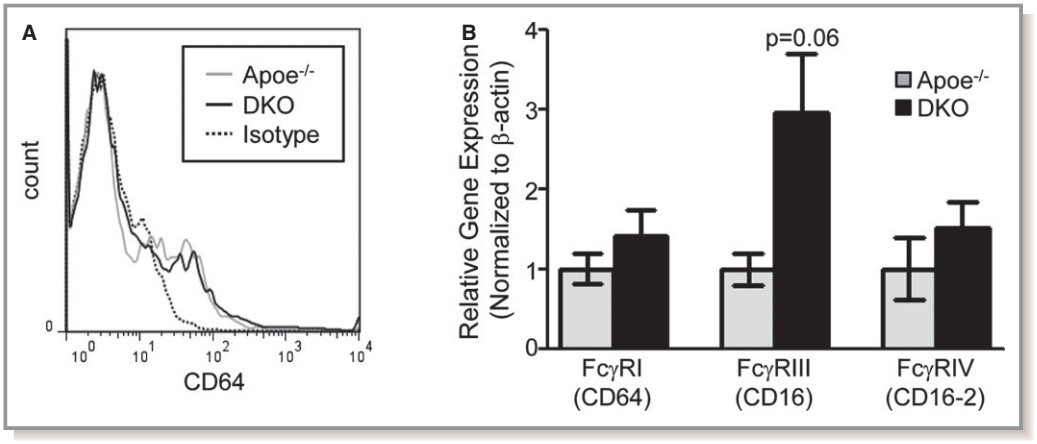

Figure 10. (A) Expression of activating FcγRs in DKO mice. Surface expression of FcγRI (CD64) on PBMCs was evaluated by flow cytometry, using an antibody to CD64 (FcγRI). CD64 levels were not different. (B) FcγRI, III, and IV transcripts were quantified by qRT-PCR from thioglycolate-elicited peritoneal macrophages (n=5). Significance was determined by independent sample *t* test. Although FcγRIII expression trended higher (P=0.06), there were no statistically significant differences in FcγR expression. Apo indicates apolipoprotein; DKO, double knockout; PBMCs, peripheral blood mononuclear cells; qRT-PCR, quantitative real-time polymerase chain reaction.

myeloid dendritic cells (mDCs; B220$^-$/CD3$^-$/CD11b$^+$/CD11c$^+$) and monocyte/macrophages (B220$^-$/CD3$^-$/CD11b$^+$/CD11c$^-$/SSC^{low}), were 2- to 3-fold higher in DKO lymph nodes (P<0.05; Table 3). MHCII expression was higher on DKO versus Apoe$^{-/-}$ mDCs (mean fluorescence intensity: 4947±677 vs. 2339±513, respectively, n=3; P<0.05), consistent with DC maturation[38] and an up-regulation that often accompanies T_{naive}→T_{reg} conversion.[39] qRT-PCR for master regulators revealed a significant increase in GATA-binding protein 3 (GATA-3) in DKOs. Although considered the T_H2 transcriptional regulator, GATA-3 is expressed by other cells types, including T_{regs}, where it plays a supporting role in T_{reg} function.[40] Given that the canonical T_H2 cytokine, IL-4, was not elevated, we conclude that GATA-3 in DKO lymph nodes is likely expressed in T_{regs}. Finally, in response to ionomycin and PMA, IL-10 trended higher (P=0.06) in DKO; no differences in IL-4, IL-12, IL-17, IFN-γ, or TGF-β were detected (Figure 11B).

In summary, DKO mice exhibit an anti-inflammatory phenotype, as evidenced by a high IgG1/IgG2a serum ratio, significantly elevated circulating IC and IL-10, and the presence of M2 MØ in plaques. The cervical lymph nodes draining the casted artery have elevated T_{regs} and antigen presenting cells. The high IC and high-fat diet likely promote the M2 MØ phenotype, as evidenced by the induction of Arg-1 upon stimulation of DKO MØ with IC and LPS. Based on multiple immunological and histological data, we conclude that removal of FcγRIIb on the Apoe$^{-/-}$ background results in skewing the immune system in an anti-inflammatory M2 direction that is atheroprotective.

Conclusions

Apoe$^{-/-}$IIb$^{-/-}$ DKO mice have reduced atherosclerosis and fibrous carotid plaques. Based on our studies[9] and those of others,[13,14] we predicted that loss of FcγRIIb would exacerbate atherosclerosis. Surprisingly, the results disproved the hypothesis, with initial evidence coming from longitudinal studies (Figure 1). Reduced plaque burden is not site specific given that DKO mice have less plaque in the carotid arteries (Figure 1), the descending aorta (Figure 2), and the aortic root (H. Ng et al, unpublished data). However, in contrast to other sites, carotid plaques are amendable to UBM, allowing for longitudinal studies. Additionally, DKO carotid plaques have many hallmarks (thick caps, few foam cells, and little necrosis) of stable human plaques. Thus, defining the mechanisms distinguishing the 2 genotypes may provide insight into why some human carotid plaques rupture while others do not.

Upon histological examination, we noted the dearth of ORO$^+$ foam cells in DKO plaques. This was not because of lack of MØ as 85% (11 of 13) of DKO plaques were CD68$^+$, and, for plaques containing MØ, the CD68/β-actin ratio was similar between the genotypes (Figure 5B). Differences in lipids may also impact the presence of foam cells. However, there were no differences in cholesterol or TG (or high-density lipoprotein-cholesterol; H. Ng et al, unpublished data) levels between the genotypes. In fact, although not statistically significant, the lipids in DKO serum trended higher (see text). Despite this, the areas of retained lipid were significantly smaller (Figure 4A), suggesting that FcγRIIb expression contributes to lipid

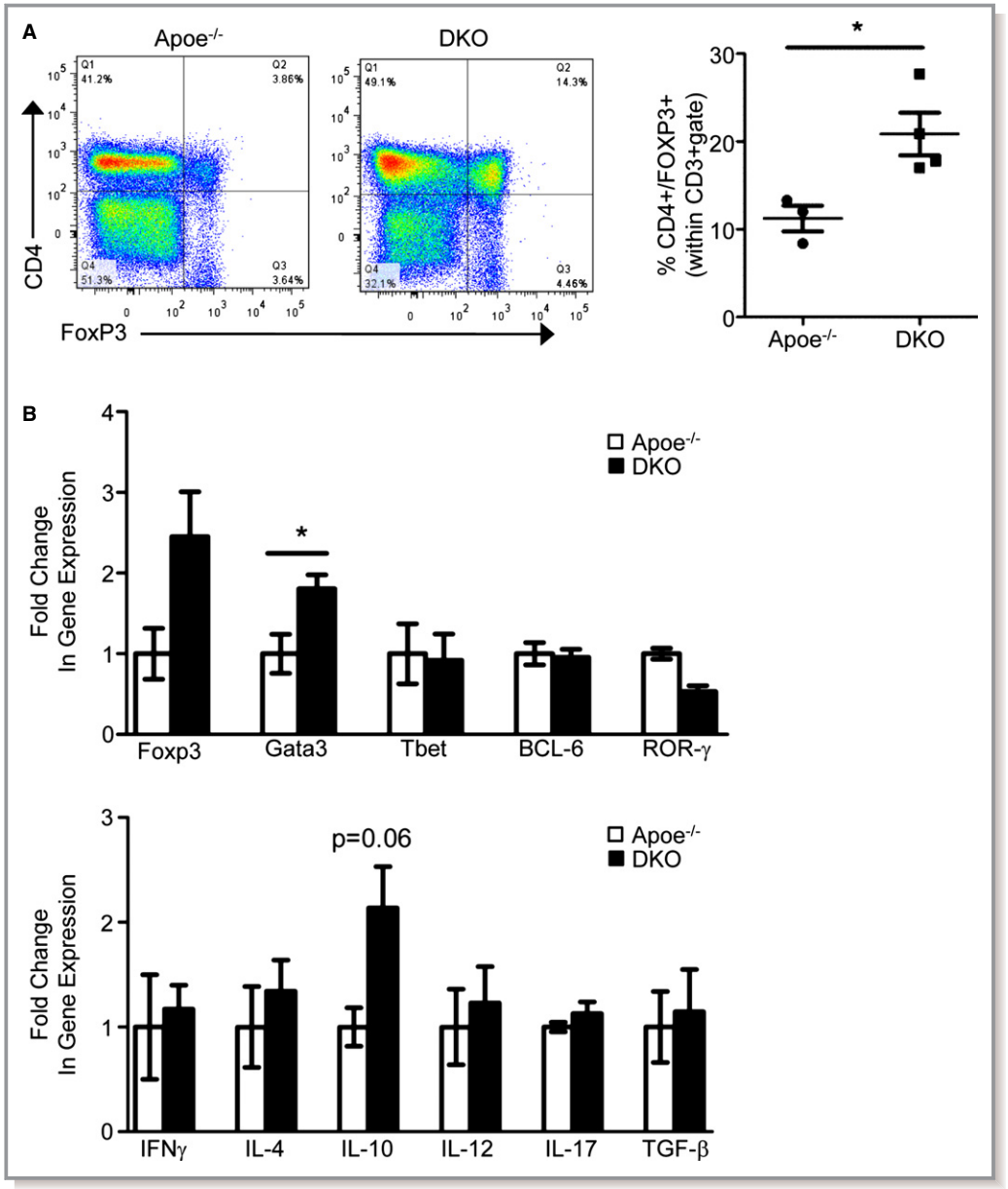

Figure 11. DKO lymph nodes are anti-inflammatory. The cervical lymph nodes draining the casted artery were stained for T_{regs} ($CD3^+CD4^+$ $Foxp3^+$) and analyzed by flow cytometry. (A) Representative plots of CD4 and Foxp3 in the $CD3^+$ gate (left) and the percentage of double positives for 3 Apoe$^{-/-}$ and 4 DKO (right). (B) qRT-PCR of lymph nodes for transcriptional regulators (top) and polarizing cytokines (bottom). Data are presented as mean±SEM (3 Apoe$^{-/-}$ and 4 DKO) lymph nodes. Apoe$^{-/-}$ white bars, DKO black bars. Significance was determined by independent sample *t* test, **P*<0.05. Apo indicates apolipoprotein; DKO, double knockout; Foxp3, forkhead box protein 3; qRT-PCR, quantitative real-time polymerase chain reaction; T_{regs}, regulatory T cells.

retention. Given that the scavenger receptors involved in lipid uptake were not significantly different (Figure 4B), it would suggest that FcγRIIb expression may influence lipid efflux. The DKO animals provide a model for studying this process.

How does loss of FcγRIIb shift the immune polarization of DKO mice? In addition to myeloid cells, FcγRIIb is expressed on B cells, where its engagement suppresses B-cell receptor signaling and regulates IgG production.[41] In its absence, IgG production continues unfettered, resulting in the elevation of both IgG and IC (Figure 8). Though mechanistic studies need to be done, we propose that elevated IgG, with IL-10 acting downstream, is driving the DKO plaque phenotype. Elevated IgG produces IC, which are significantly higher in DKO serum (Figure 8). IC, combined with TLR4 ligands (saturated fatty acids derived

Table 3. Cell Composition in the Lymph Nodes of Apoe$^{-/-}$ and DKO Mice

Cervical Lymph Nodes	Apoe$^{-/-}$ (n=8)	DKO (n=7)
B220^{+}/CD3^{-}	39.5±3.1	43.9±4.5
CD3^{+}/B220^{-}	38.0±4.5	29.6±2.5
CD4^{+}/CD8$^{-\dagger}$	49.8±0.8	56.6±2.3*
CD8^{+}/CD4$^{-\dagger}$	38.0±1.9	28.8±1.0**
CD11c^{+}/CD11b^{+}/CD3^{-}/B220^{-}	0.48±0.1	1.3±0.4*
CD11c^{-}/CD11b^{+}/CD3^{-}/B220^{-}/SSC^{hi}	0.5±0.1	0.6±0.1
CD11c^{-}/CD11b^{+}/CD3^{-}/B220^{-}/SSC^{low}	0.5±0.1	0.9±0.1*

Cervical lymph nodes draining the casted artery were removed at 26 weeks and the cells analyzed by flow cytometry. Data are presented as mean±SEM percent of the total cell population and analyzed by independent sample *t* test. Apo indicates apolipoprotein; DKO, double knockout.

*P<0.05; **P<0.01. CD4^{+} T cells were increased with a corresponding decrease in CD8^{+} cells. Myeloid-derived dendritic cells were also significantly elevated in DKO lymph nodes.

†Percent of CD3^{+} population.

from the Western diet[32,33]) produce M2b MØ, which express Arg-1 (Figures 6A and 9A) and produce IL-10 (Figure 9 and previous work[17]). Two features of high-circulating IgG may contribute to the anti-inflammatory DKO environment. The Ravetch lab has reported on the anti-inflammatory nature of sialylated IgG[42–44] that act through MØ to reduce the arthritis model and are the active component of the anti-inflammatory effects of IVIg.[43] Although a minor component of IgG, their absolute concentration in DKO serum is likely elevated in proportion to the overall 2-fold increase in IgG levels (Figure 8). Second, it has been reported that the constant fragment of IgG contains MHC-binding epitopes ("Tregitopes") that, when incubated with peripheral blood mononuclear cells (PBMCs), activate T_{regs} and induce IL-10 expression.[45] The draining lymph nodes of DKO mice have elevated antigen-presenting cells (mDCs and MØ; Table 3) that could present Tregitopes (higher in DKOs as a result of IgG levels; Figure 8) to naïve T cells, producing the T_{regs} that are enriched in DKO lymph nodes (Figure 11) and spleen (see H. Ng et al, unpublished data). T_{regs} and M2 MØ release IL-10, and we have data demonstrating that IL-10 is preferentially produced by DKO versus Apoe$^{-/-}$ CD4^{+} splenocytes (see H. Ng et al, unpublished data). Thus, DKO blood, spleen, and lymph nodes contain the factors for polarizing M2b (IC+TLR4 ligand) and M2c MØ (IL-10 from T_{regs} and/or M2b MØ). Although we did not stain plaques for T_{regs}, their presence in the lymph nodes is suggestive of their expression in DKO plaques. However, direct evidence for M2 skewing in DKO animals is the expression of Arg-1 in plaque MØ (Figure 6) and its up-regulation in DKO MØ treated with IC and LPS (Figure 9).

Why Do These Results Differ From Other DKO Atherosclerosis Reports?

The results disproved our hypothesis and are in direct contrast to the literature.[13,14] The differences may arise from the extent of backcrossing in the FcγRIIb knockout mice used to generate the DKOs. Specifically, the FcγRIIb$^{-/-}$ mice used to generate the Apoe$^{-/-}$ FcγRIIb$^{-/-}$ DKO used in the published report[13] were strain 002848 (The Jackson Laboratory), a mixture of C57BL/6 and 129S. Single-nucleotide polymorphism analyses confirmed that the 002848 strain is ≈50% 129S, whereas the Taconic FcγRIIb$^{-/-}$ strain #580 is greater than 95% C57BL/6 (see H. Ng et al, unpublished data). Thus, the genetic background of our mice is predominantly C57/BL6 ("congenic"), whereas that of the mice from the other group[13] are on a mixed background. "Mixed" versus congenic DKO mice produce diametrically opposite results, with the mixed background exhibiting proinflammatory skewing and the congenic mice (used in this study) being anti-inflammatory. Notably, others have documented a similar FcγRIIb congenic versus mixed disparity in a lupus model and determined that, similar to these atherosclerosis results, the mixed DKO are susceptible to lupus, whereas the congenic DKO are protected.[46]

The reader is directed to our second article (H. Ng et al, unpublished data) for additional studies on reduced atherosclerosis in this DKO mouse. The 2 articles use different atherosclerotic sites, diets, and age, demonstrating that the protective environment is a general feature of high-fat-diet–fed congenic FcγRIIb/Apoe DKO mice. Additionally, whereas the focus of the present manuscript defines the histological differences in carotid plaques of Apoe$^{-/-}$ and DKO mice, the polarization of the macrophages in the plaques, and immune composition of the lymph nodes, the companion article (H. Ng et al, unpublished data) establishes that the protective environment of the DKO animals derives from the congenic background of the mice. In that article, the responses of macrophages from mixed and congenic background DKO mice were directly compared and shown to be pro- and anti-inflammatory, respectively, with the protective phenotype a function of the congenic background.

The results detailed herein advance our understanding of the mechanisms underlying the development of stable plaques. That the model has translational potential is apparent from studies reporting that humans that have elevated levels of IL-10 and T_{regs} develop less-vulnerable plaques.[37]

Acknowledgments

The authors thank Christina Rotundi in the AMC histology core for CD68 staining, Jocelyn Laboy for developing the Oil Red O quantitation protocol, Tabassum Rahman and Anothony Francini for

running the Luminex® arrays, Danielle Califano for advising with flow cytometry, and Casey O'Connor for assisting with data collection. The authors also thank Daniel Loegering and Antonio Paul for their insight and suggestions regarding the project and James Drake and Edmund Gosselin for critical reading of the manuscript. The authors thank Rosemary Naftalis and Debbie Moran for putting together the figures.

Sources of Funding

This work was supported by NIH HL095971, HL089730, and GM09032507 (Lennartz), R01 HL086674 (Nagarajan), and a seed grant from The Albany Medical College Research Grant Bridge Program (Lennartz).

Disclosures

None.

References

1. Roger VL, Go AS, Lloyd-Jones DM, Benjamin EJ, Berry JD, Borden WB, Bravata DM, Dai S, Ford ES, Fox CS, Fullerton HJ, Gillespie C, Hailpern SM, Heit JA, Howard VJ, Kissela BM, Kittner SJ, Lackland DT, Lichtman JH, Lisabeth LD, Makuc DM, Marcus GM, Marelli A, Matchar DB, Moy CS, Mozaffarian D, Mussolino ME, Nichol G, Paynter NP, Soliman EZ, Sorlie PD, Sotoodehnia N, Turan TN, Virani SS, Wong ND, Woo D, Turner MB. Heart disease and stroke statistics–2012 update: a report from the American Heart Association. *Circulation*. 2012;125:e2–e220.
2. Devuyst G, Karapanayiotides T, Ruchat P, Pusztaszeri M, Lobrinus JA, Jonasson L, Cuisinaire O, Kalangos A, Despland PA, Thiran JP, Bogousslavsky J. Ultrasound measurement of the fibrous cap in symptomatic and asymptomatic atheromatous carotid plaques. *Circulation*. 2005;111:2776–2782.
3. von der Thusen JH, van Berkel TJ, Biessen EA. Induction of rapid atherogenesis by perivascular carotid collar placement in apolipoprotein E-deficient and low-density lipoprotein receptor-deficient mice. *Circulation*. 2001;103:1164–1170.
4. Cheng C, van Haperen R, de Waard M, van Damme LC, Tempel D, Hanemaaijer L, van Cappellen GW, Bos J, Slager CJ, Duncker DJ, van der Steen AF, de Crom R, Krams R. Shear stress affects the intracellular distribution of eNOS: direct demonstration by a novel in vivo technique. *Blood*. 2005;106:3691–3698.
5. Cheng C, Tempel D, van Haperen R, van der Baan A, Grosveld F, Daemen MJ, Krams R, de Crom R. Atherosclerotic lesion size and vulnerability are determined by patterns of fluid shear stress. *Circulation*. 2006;113:2744–2753.
6. Helderman F, Segers D, de Crom R, Hierck BP, Poelmann RE, Evans PC, Krams R. Effect of shear stress on vascular inflammation and plaque development. *Curr Opin Lipidol*. 2007;18:527–533.
7. Harmon EY, Fronhofer V, Keller RS, Feustel PJ, Brosnan MJ, von der Thüsen JH, Loegering DJ, Lennartz MR. Ultrasound biomicroscopy for longitudinal studies of carotid plaque development in mice: validation with histological endpoints. *PLoS One*. 2012;7:e29944.
8. Libby P, Ridker PM, Hansson GK. Inflammation in atherosclerosis: from pathophysiology to practice. *J Am Coll Cardiol*. 2009;54:2129–2138.
9. Lennartz MR, Aggarwal A, Michaud TM, Feustel PJ, Jones DM, Brosnan MJ, Keller RS, Loegering DJ, Kreienberg PB. Ligation of macrophage Fcγ receptors recapitulates the gene expression pattern of vulnerable human carotid plaques. *PLoS One*. 2011;6:e21803.
10. Ng HP, Burris RL, Nagarajan S. Attenuated atherosclerotic lesions in apoE-Fcgamma chain-deficient hyperlipidemic mouse model is associated with inhibition of Th17 cells and promotion of regulatory T cells. *J Immunol*. 2011;187:6082–6093.
11. Hernandez-Vargas P, Ortiz-Munoz G, Lopez-Franco O, Suzuki Y, Gallego-Delgado J, Sanjuan G, Lazaro A, Lopez-Parra V, Ortega L, Egido J, Gomez-Guerrero C. Fcgamma receptor deficiency confers protection against atherosclerosis in apolipoprotein E knockout mice. *Circ Res*. 2006;99:1188–1196.
12. Kelly JA, Griffin ME, Fava RA, Wood SG, Bessette KA, Miller ER, Huber SA, Binder CJ, Witztum JL, Morganelli PM. Inhibition of arterial lesion progression in CD16-deficient mice: evidence for altered immunity and the role of IL-10. *Cardiovasc Res*. 2010;85:224–231.
13. Mendez-Fernandez YV, Stevenson BG, Diehl CJ, Braun NA, Wade NS, Covarrubias R, van Leuven S, Witztum JL, Major AS. The inhibitory Fc [gamma]RIIb modulates the inflammatory response and influences atherosclerosis in male apoE-/- mice. *Atherosclerosis*. 2011;214:73–80.
14. Zhao M, Wigren M, Duner P, Kolbus D, Olofsson KE, Bjorkbacka H, Nilsson J, Fredrikson GN. Fc{gamma}RIIB inhibits the development of atherosclerosis in low-density lipoprotein receptor-deficient mice. *J Immunol*. 2010;184:2253–2260.
15. Gallo P, Goncalves R, Mosser DM. The influence of IgG density and macrophage Fc (gamma) receptor cross-linking on phagocytosis and IL-10 production. *Immunol Lett*. 2010;133:70–77.
16. Khallou-Laschet J, Varthaman A, Fornasa G, Compain C, Gaston AT, Clement M, Dussiot M, Levillain O, Graff-Dubois S, Nicoletti A, Caligiuri G. Macrophage plasticity in experimental atherosclerosis. *PLoS One*. 2010;5:e8852.
17. Mantovani A, Sica A, Sozzani S, Allavena P, Vecchi A, Locati M. The chemokine system in diverse forms of macrophage activation and polarization. *Trends Immunol*. 2004;25:677–686.
18. Hansson GK, Hermansson A. The immune system in atherosclerosis. *Nat Immunol*. 2011;12:204–212.
19. Libby P, Lichtman AH, Hansson GK. Immune effector mechanisms implicated in atherosclerosis: from mice to humans. *Immunity*. 2013;38:1092–1104.
20. Seimon TA, Wang Y, Han S, Senokuchi T, Schrijvers DM, Kuriakose G, Tall AR, Tabas IA. Macrophage deficiency of p38alpha MAPK promotes apoptosis and plaque necrosis in advanced atherosclerotic lesions in mice. *J Clin Invest*. 2009;119:886–898.
21. Kuchibhotla S, Vanegas D, Kennedy DJ, Guy E, Nimako G, Morton RE, Febbraio M. Absence of CD36 protects against atherosclerosis in ApoE knock-out mice with no additional protection provided by absence of scavenger receptor A I/II. *Cardiovasc Res*. 2008;78:185–196.
22. Stary HC, Chandler AB, Dinsmore RE, Fuster V, Glagov S, Insull W Jr, Rosenfeld ME, Schwartz CJ, Wagner WD, Wissler RW. A definition of advanced types of atherosclerotic lesions and a histological classification of atherosclerosis. A report from the Committee on Vascular Lesions of the Council on Arteriosclerosis, American Heart Association. *Arterioscler Thromb Vasc Biol*. 1995;15:1512–1531.
23. Moore KJ, Tabas I. Macrophages in the pathogenesis of atherosclerosis. *Cell*. 2011;145:341–355.
24. Libby P. Inflammation in atherosclerosis. *Nature*. 2002;420:868–874.
25. Chinetti-Gbaguidi G, Baron M, Bouhlel MA, Vanhoutte J, Copin C, Sebti Y, Derudas B, Mayi T, Bories G, Tailleux A, Haulon S, Zawadzki C, Jude B, Staels B. Human atherosclerotic plaque alternative macrophages display low cholesterol handling but high phagocytosis because of distinct activities of the PPAR{gamma} and LXRα Pathways. *Circ Res*. 2011;108:985–995.
26. Boyle JJ, Johns M, Kampfer T, Nguyen AT, Game L, Schaer DJ, Mason JC, Haskard DO. Activating transcription factor 1 directs Mhem atheroprotective macrophages through coordinated iron handling and foam cell protection. *Circ Res*. 2012;110:20–33.
27. Mantovani A, Garlanda C, Locati M. Macrophage diversity and polarization in atherosclerosis: a question of balance. *Arterioscler Thromb Vasc Biol*. 2009;29:1419–1423.
28. Liu Y, Li D, Chen J, Xie J, Bandyopadhyay S, Zhang D, Nemarkommula AR, Liu H, Mehta JL, Hermonat PL. Inhibition of atherogenesis in LDLR knockout mice by systemic delivery of adeno-associated virus type 2-hIL-10. *Atherosclerosis*. 2006;188:19–27.
29. Potteaux S, Esposito B, van Oostrom O, Brun V, Ardouin P, Groux H, Tedgui A, Mallat Z. Leukocyte-derived interleukin 10 is required for protection against atherosclerosis in low-density lipoprotein receptor knockout mice. *Arterioscler Thromb Vasc Biol*. 2004;24:1474–1478.
30. Caligiuri G, Rudling M, Ollivier V, Jacob MP, Michel JB, Hansson GK, Nicoletti A. Interleukin-10 deficiency increases atherosclerosis, thrombosis, and low-density lipoproteins in apolipoprotein E knockout mice. *Mol Med*. 2003;9:10–17.
31. Nimmerjahn F, Ravetch JV, Frederick WA. Fc-receptors as regulators of immunity. In: Frederick ALT, ed. *Advances in Immunology*. Waltham, MA: Academic Press; 2007:179–204.
32. Lee JY, Sohn KH, Rhee SH, Hwang D. Saturated fatty acids, but not unsaturated fatty acids, induce the expression of cyclooxygenase-2 mediated through Toll-like receptor 4. *J Biol Chem*. 2001;276:16683–16689.

33. Lee JY, Ye J, Gao Z, Youn HS, Lee WH, Zhao L, Sizemore N, Hwang DH. Reciprocal modulation of Toll-like receptor-4 signaling pathways involving MyD88 and phosphatidylinositol 3-kinase/AKT by saturated and polyunsaturated fatty acids. *J Biol Chem*. 2003;278:37041–37051.

34. Larsen EC, Ueyama T, Brannock PM, Shirai Y, Saito N, Larsson C, Loegering D, Weber PB, Lennartz MR. A role for PKC-varepsilon in FcgammaR-mediated phagocytosis by RAW 264.7 cells. *J Cell Biol*. 2002;159:939–944.

35. Klingenberg R, Gerdes N, Badeau RM, Gistera A, Strodthoff D, Ketelhuth DF, Lundberg AM, Rudling M, Nilsson SK, Olivecrona G, Zoller S, Lohmann C, Luscher TF, Jauhiainen M, Sparwasser T, Hansson GK. Depletion of FOXP3+ regulatory T cells promotes hypercholesterolemia and atherosclerosis. *J Clin Invest*. 2013;123:1323–1334.

36. Mor A, Planer D, Luboshits G, Afek A, Metzger S, Chajek-Shaul T, Keren G, George J. Role of naturally occurring CD4+ CD25+ regulatory T cells in experimental atherosclerosis. *Arterioscler Thromb Vasc Biol*. 2007;27:893–900.

37. George J, Schwartzenberg S, Medvedovsky D, Jonas M, Charach G, Afek A, Shamiss A. Regulatory T cells and IL-10 levels are reduced in patients with vulnerable coronary plaques. *Atherosclerosis*. 2012;222:519–523.

38. Kalergis AM, Ravetch JV. Inducing tumor immunity through the selective engagement of activating Fcgamma receptors on dendritic cells. *J Exp Med*. 2002;195:1653–1659.

39. Rutella S, Danese S, Leone G. Tolerogenic dendritic cells: cytokine modulation comes of age. *Blood*. 2006;108:1435–1440.

40. Wang Y, Su MA, Wan YY. An essential role of the transcription factor GATA-3 for the function of regulatory T cells. *Immunity*. 2011;35:337–348.

41. Nimmerjahn F, Ravetch JV. Fcgamma receptors: old friends and new family members. *Immunity*. 2006;24:19–28.

42. Kaneko Y, Nimmerjahn F, Ravetch JV. Anti-inflammatory activity of immunoglobulin G resulting from Fc sialylation. *Science*. 2006;313:670–673.

43. Anthony RM, Ravetch JV. A novel role for the IgG Fc glycan: the anti-inflammatory activity of sialylated IgG Fcs. *J Clin Immunol*. 2010;30(suppl 1): S9–S14.

44. Anthony RM, Kobayashi T, Wermeling F, Ravetch JV. Intravenous gammaglobulin suppresses inflammation through a novel T(H)2 pathway. *Nature*. 2011;475:110–113.

45. De Groot AS, Moise L, McMurry JA, Wambre E, Van Overtvelt L, Moingeon P, Scott DW, Martin W. Activation of natural regulatory T cells by IgG Fc-derived peptide "Tregitopes". *Blood*. 2008;112:3303–3311.

46. Boross P, Arandhara VL, Martin-Ramirez J, Santiago-Raber ML, Carlucci F, Flierman R, van der Kaa J, Breukel C, Claassens JW, Camps M, Lubberts E, Salvatori D, Rastaldi MP, Ossendorp F, Daha MR, Cook HT, Izui S, Botto M, Verbeek JS. The inhibiting Fc receptor for IgG, FcgammaRIIB, is a modifier of autoimmune susceptibility. *J Immunol*. 2011;187:1304–1313.